

PAPER View Article Online
View Journal | View Issue



Cite this: *Soft Matter,* 2020, **16**. 1287

The interplay of thermodynamics and kinetics: imparting hierarchical control over film formation of self-stratified blends†

Samantha J. Rinehart, Da Guangcui Yuan and Mark D. Dadmun xad

Spin casting has become an attractive method to fabricate polymer thin films found in organic electronic devices such as field-effect transistors, and light emitting diodes. Many studies have shown that altering spin casting parameters can improve device performance, which has been directly correlated to the degree of polymer alignment, crystallinity, and morphology of the thin film. To provide a thorough understanding of the balance of thermodynamic and kinetic factors that influence the stratification of polymer blend thin films, we monitor stratified polymer blend thin films developed from poly-(3-hexylthiophene-2,5-diyl) and poly(methyl methacrylate) blends at controlled loading ratios, relative molecular weights, and casting speed. The structures of these thin films were characterized via neutron reflectivity, and the results show that at the fastest casting speed, polymer-polymer interactions and surface energy of the polymers in the blend dictate the final film structure, and at the slowest casting speed, there is less control over the film layering due to the polymer-polymer interactions, surface energy, and entropy simultaneously driving stratification. As well, the relative solubility limits of the polymers in the pre-deposition solution play a role in the stratification process at the slowest casting speed. These results broaden the current understanding of the relationship between spin casting conditions and vertical phase separation in polymer blend thin films and provide a foundation for improved rational design of polymer thin film fabrication processes to attain targeted stratification, and thus performance.

Received 7th June 2019, Accepted 30th December 2019

DOI: 10.1039/c9sm01147a

rsc.li/soft-matter-journal

Introduction

Spin casting has been used for multiple decades as a method to fabricate polymer thin films that are as thick as 50 microns to as thin as a few nanometers. It is well known that casting speed, solution loading, and polymer molecular weight have an effect on final film thickness. Phin casting has become an attractive deposition method for the fabrication of films for many applications ranging from organic electronic devices to a variety of polymer coatings. Pecifically in the device fabrication field, careful modification of the spin casting processing parameters such as solvent, casting speed, and polymer loading elicit various qualitative trends in polymer gelation, crystallization, and chain alignment. Per section of the spin casting speed.

Recently, devices with improved performance and durability have been realized by fabricating from solutions of polymer blends. 14-17 Typically each polymer in the blend is soluble in a common solvent which allows for one-step solution processing, streamlining the fabrication process. 14,17 Additionally, polymer blends open the possibility of auto-assembly or self-stratification into useful structures with practical interfaces for organic electronics. 18-20 As with spin casting single-component polymer solutions, the morphology of a polymer blend final film is dictated by the deposition conditions. However, the relationship between spin casting conditions and structure formation in the fabricated film becomes more complex with the addition of another polymer. 21-23 The concurrent and competing interactions between the two polymers, between polymers and solvent, and between polymers and substrate result in a complex process where it is difficult to anticipate and predict the final film structure.24 This limits the ability to rationally alter the spin casting conditions to design the final device structure to a targeted morphology, which is detrimental to rationally improving device performance by directing final film architecture.²⁵

The various binary interactions present in the deposition process of polymer blend films are known, yet the importance of each interaction in the deposition process and its contribution

^a Department of Chemistry, University of Tennessee, Knoxville, Tennessee 37996, USA. E-mail: Dad@utk.edu

b NIST Center for Neutron Research, National Institute of Standards and Technology, Gaithersburg, Maryland 20899, USA

^c University of Georgetown, Washington, D.C. 20057, USA

^d Chemical Sciences Division, Oak Ridge National Laboratory, Oak Ridge, Tennessee 37830. USA

 $[\]dagger$ Electronic supplementary information (ESI) available. See DOI: 10.1039/ c9sm01147a

towards final film structure is less understood.²⁵ Self-stratification

Paper

towards final film structure is less understood.²³ Self-stratification is a term used to encompass the vertical phase separation of polymer blends in thin films and is widely accepted as a thermodynamically driven process despite intrinsic kinetic trapping effects.²⁶ Kinetic trapping occurs during the short time scales of spin-cast film formation and prevents the blend film from reaching its equilibrium. Many studies have demonstrated varying device performance with a change in casting solvent.^{8-10,27} However, the variation in device performance is often attributed to polymer-solvent or specific surface energy interactions; yet the impact of solvent evaporation rate and kinetics of film formation are often overlooked.

To address these shortcomings, our group has studied the dominating driving forces of film formation and stratification of poly(3-hexylthiophene-2,5-diyl) (P3HT) and poly(methyl methacrylate) (PMMA) blends by monitoring the final film structure as a function of processing conditions, including casting speed, blend composition, and polymer molecular weight.²⁸ These experiments reveal that as polymer molecular weight and blend composition were altered, thermodynamic interactions such as polymer surface energy, and the polymerpolymer interaction parameter controlled final film stratification. Additionally, the kinetic and thermodynamic effects on final film structure were decoupled by controlling casting speed to vary film formation time, rather than introducing a more slowly drying solvent, which also alters the thermodynamic interactions of the system. By keeping all thermodynamic parameters constant, the kinetic effects on final film structure are isolated. The kinetics of spin casting was monitored in-situ with light reflectivity during the film formation process. The results of film formation time paired with the final thin film structure showed that the longer film formation time of slower casting speeds resulted in larger extents of stratification relative to the samples prepared at fast casting speeds. We attribute this increased layering to the fact that the fully stratified film is the thermodynamic endpoint, and longer film formation time allows the film to evolve closer towards this equilibrium.

The work describe here expands the solution and casting parameters including blend composition, polymer molecular weight, and casting speed, to gain an increased understanding of the impact of each thermodynamic parameter on the stratification process, and provide a foundation that can aid in the development of guidelines to rationally design and tune the stratification in polymer blend films simply by altering predeposition solution properties and processing conditions.

Experimental

Chlorobenzene (Sigma Aldrich), poly(3-hexylthiophene-2,5-diyl) (P3HT) (Ossila, regioregularity-95%, and number-average molecular weight ($M_{\rm n}$) 19 500 g mol $^{-1}$ and polydispersity index (PDI) 1.75) and deuterated poly(methyl methacrylate (dPMMA)) (Polymer Source Inc., $M_{\rm n}$ (PDI), 20 000 g mol $^{-1}$ (1.6), 131 500 g mol $^{-1}$ (1.4), 316 000 g mol $^{-1}$ (1.35), 520 000 g mol $^{-1}$ (1.4)) were used directly from the supplier and were not further purified.

Polymer blends were dissolved at 1 percent by weight in ratios of P3HT: dPMMA 5:95, 10:90, 15:85, 20:80 in chlorobenzene at 55 °C overnight. Thin films were prepared by spin coating (209.4 rad s $^{-1}$ or 52.4 rad s $^{-1}$) the chlorobenzene solutions onto Si wafers (previous results analyzed a middle casting speed, 104.7 rad s $^{-1}$). The Si wafers were cleaned in a piranha solution (1:3 ratio of sulfuric acid and hydrogen peroxide), washed with nanopure water, and placed under UV irradiation and ozone.

Neutron reflectivity experiments were conducted at the National Institute of Standards and Technology's Center for Neutron Research (NCNR) using the NG7 beamline with a Q range of 0.008–0.2 A^{-1} where $Q = 4\pi/\lambda \sin(\theta)$; λ is the neutron wavelength, and θ is the angle of incidence. The data for all incident angles was reduced utilizing the NCNR software.

The solubility limits of protonated poly(methyl methacry-late) (H-PMMA) in chlorobenzene were determined using transmission infrared spectroscopy (IR). H-PMMA was obtained from Acros (M_n 15 000 g mol⁻¹), Sigma-Aldrich (weight average molecular weight (M_w) 120 000 g mol⁻¹ and 350 000 g mol⁻¹), and M_n 520 000 g mol⁻¹ dPMMA was obtained from Polymer Source. IR spectra were recorded with a Thermo Scientific Nicolet iS50 FTIR Spectrometer and a transmission cell. The solubility limits for H-PMMA and dPMMA were determined by monitoring the intensity of the carbonyl peak (1730 cm⁻¹) (A) combined with the Beer–Lambert law (eqn (1)) where c is the concentration of the solution, ε is the molar absorptivity, and l is the path-length.

$$A = c\varepsilon l$$
 (1)

The molar absorptivity was determined by measuring the intensity of the carbonyl peak for each molecular weight of H-PMMA and dPMMA at known concentrations and plotted as a function of PMMA concentration. The slope of the line from each of these graphs is the molar absorptivity. A separate saturated solution for each molecular weight was made, filtered, and serially diluted. The serial dilution is necessary because the detector cannot detect such high carbonyl absorption. The intensity of the carbonyl peak is obtained for each of the dilutions, compared to the Beer-Lambert Plot to determine the concentration, and then this concentration is multiplied by the dilution factor to determine the solubility limit. The P3HT solubility limit in chlorobenzene was obtained by following a similar procedure except with the use of a Thermo Scientific Evolution 300 UV-vis spectrophotometer and monitoring the intensity of the 457 nm peak.

Results and discussion

The effects of blend composition of P3HT: dPMMA (5:95, 10:90, 15:85, or 20:80), dPMMA molecular weight (20000 g mol⁻¹, 131 500 g mol⁻¹, 316 000 g mol⁻¹, or 520 000 g mol⁻¹) and casting speed (209.4 rad s⁻¹, 104.7 rad s⁻¹, or 52.4 rad s⁻¹) on thin film vertical structure were examined *via* neutron reflectivity. Neutron reflectivity provides a normalized reflection profile as a function of incident wave vector, Q. The neutron reflectivity data was

fit using IGOR and Motofit software packages using a multi-layer model. The analysis provides a scattering length density (SLD) depth profile with the restraint that the SLD depth profile must adhere within 5% to the known composition of the sample. The SLD depth profile from each sample was transformed into a P3HT volume fraction as a function of the normalized thickness, where 0 denotes the air interface to 1 denotes the ${\rm SiO}_2$ interface. The normalization of thickness allows a more direct comparison among the films formed from all casting speeds and polymer

molecular weights. The transformation into the P3HT volume

fraction transpires by employing eqn (2):

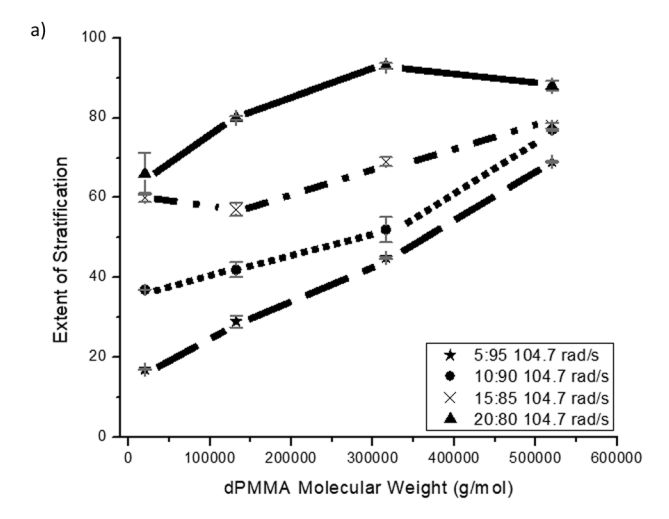
$$\frac{\mathrm{SLD}_{\mathrm{layer}}(z) - \mathrm{SLD}_{\mathrm{dPMMA}}}{\mathrm{SLD}_{\mathrm{dPMMA}} - \mathrm{SLD}_{\mathrm{P3HT}}} = \phi_{\mathrm{P3HT}}(z) \tag{2}$$

where $SLD_{layer}(z)$ is the SLD of the sample at depth z, and $\phi_{P3HT}(z)$ is the volume fraction of P3HT at depth z. The SLDs of P3HT and dPMMA were calculated from the NCNR SLD calculator. The SLD values used throughout these experiments are $0.7 \times 10^{-6} \, \text{Å}^{-2}$ and a range of $6.7 \times 10^{-6} \, \text{Å}^{-2}$ – $7.1 \times 10^{-6} \, \text{Å}^{-2}$ for P3HT and the range of molecular weights of dPMMA, respectively.

The P3HT volume fraction depth profiles can be utilized to determine the quantitative measure of the extent of stratification of each sample. The extent of stratification is determined by employing a previously described method. In this method, the extent of stratification of a two-component system is compared to two theoretical limits: a homogenous (0%, non-stratified) thin film and a completely stratified (100%, two independently pure layers) thin film. The extent of stratification value obtained by this analysis quantifies the extent of vertical phase separation of the two components. For example, a thin film sample containing a 50/50 blend of two polymers is defined as stratified if any sub-layer contains more than 50% of either polymer. A sub-layer is defined as any thickness within the thin film smaller than the total thickness of the film where the sum of all the sub-layers equals the total film thickness.

Our previous studies of the stratification in spin-coated films investigated the impact of PMMA molecular weight at a single spin speed (104.7 rad s⁻¹, Fig. 1a) as well as the impact of casting speed at a single PMMA molecular weight $(131500 \text{ g mol}^{-1})$ Fig. 1b) on the layered structure of the fabricated P3HT/dPMMA films. These results show that as the dPMMA molecular weight decreased, a decrease of extent of stratification was observed for all blend compositions prepared at 104.7 rad s⁻¹. In addition, as the P3HT concentration in the blend increased, the extent of stratification increased regardless of the molecular weight of dPMMA or casting speed used in the preparation of the sample. Moreover, the casting speed did not alter the variation in stratification of samples formed from high or low loadings of P3HT in the blend, vet a sample cast with a slower casting speed resulted in a larger extent of stratification relative to the same sample prepared at faster casting speeds.28

The previous study examined each parameter independently and cannot speak to their relative importance on stratification. To more accurately define the relative importance of these factors in determining the extent of stratification in spin cast polymer blend thin films, we have expanded our studies to investigate thin films



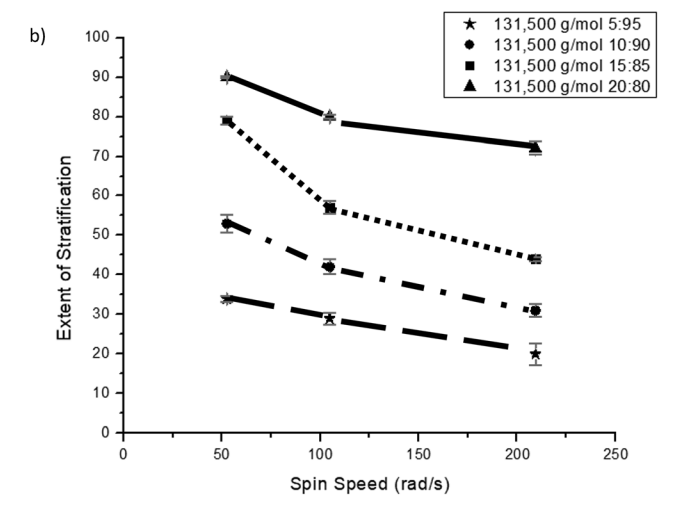


Fig. 1 (a) A previously reported plot of extent of stratification as a function of dPMMA molecular weight and blend composition 5:95 (stars), 10:90 (circles), 15:85 (crosses), and 20:80 (triangles) all prepared at $104.7 \, {\rm rad \, s^{-1}}$. (b) Plot of extent of stratification as a function of spin cast speed, and blend composition 5:95 (stars), 10:90 (circles), 15:85 (crosses), and 20:80 (triangles) all prepared with $131500 \, {\rm g \, mol^{-1}} \, {\rm dPMMA}$.

consisting of P3HT:dPMMA blends (5:95, 10:90, 15:85, 20:80), with one of three dPMMA molecular weights (20000 g mol⁻¹, 316 000 g mol⁻¹, 520 000 g mol⁻¹), prepared at one of three casting speeds (209.4 rad s⁻¹, 104.7 rad s⁻¹, 52.4 rad s⁻¹). The impact of molecular weight and P3HT concentration at each casting speed will be discussed first and then the impact of molecular weight over the range of casting speeds is discussed. It is important to note that all of the samples investigated in this manuscript and the respective discussions are as-cast films and none of these samples have been annealed in any way.

209.4 rad s⁻¹ casting speed preparation

dPMMA molecular weight. Fig. 2 plots the extent of stratification of the fabricated films as a function of dPMMA molecular weight for samples containing four different blend compositions all cast at 209.4 rad s⁻¹. The samples consisting of blend compositions of P3HT:dPMMA 10:90, 15:85, and

Paper

* 5:95 209.4 rad/s

10:90 209.4 rad/s

10:90 209.4 rad/s

15:85 209.4 rad/s

20:80 209.4 rad/s

20:80 209.4 rad/s

Fig. 2 Plot of extent of stratification as a function of dPMMA molecular weight, and blend composition 5:95 (stars), 10:90 (circles), 15:85 (crosses), and 20:80 (triangles) all prepared at 209.4 rad s⁻¹.

dPMMA Molecular Weight (g/mol)

20:80 prepared at 209.4 rad s⁻¹ elicit a decrease in extent of stratification as the molecular weight of dPMMA decreases, although the impact of molecular weight on stratification is minimal relative to the samples prepared at 104.7 rad s $^{-1}$. This change may be attributed to the film formation time, where the samples prepared at 209.4 $\rm rad~s^{-1}$ have a shorter film formation time than those made at 104.7 rad s^{-1} . We attributed the stratification of the samples prepared at 104.7 rad s⁻¹ to the entropic surface segregation of the smaller P3HT chains (i.e. an entropic phase separation) during the slightly longer film formation time. Due to the shorter film formation time of the 209.4 rad s⁻¹ samples, we believe that there is not ample time for the smaller P3HT chains to stratify in the spin casting process. Since chain end concentration correlates to the amount of entropy in the system, our results indicate that entropy plays a reduced role in the final film structure when samples are prepared at 209.4 rad s⁻¹, relative to when samples are prepared at 104.7 rad s⁻¹. However, the extents of stratification for all P3HT:20 000 g mol⁻¹ dPMMA blends are significantly reduced relative to the blends containing larger molecular weight dPMMA. P3HT (~20000 g mol⁻¹) and 20000 g mol⁻¹ dPMMA have similar molecular weights. Considering each polymer contributes a similar amount of entropy to the system, the entropic contribution would not drive de-mixing of the two polymers. Therefore, entropy plays a reduced role in driving stratification when samples are prepared at 209.4 rad s⁻¹ relative to slower casting speeds.

It is interesting to note that the samples consisting of P3HT: dPMMA 5:95 show an increase in extent of stratification as a function of decreased dPMMA molecular weight from $520\,000~\mathrm{g}~\mathrm{mol}^{-1}$ to $131\,500~\mathrm{g}~\mathrm{mol}^{-1}$ rather than a decrease as seen with the other blend compositions. This trend will be discussed in more detail in another part of the text.

P3HT concentration. At 209.4 rad s⁻¹, the extent of stratification increases as the P3HT concentration increases in the blends for all dPMMA molecular weights, except the smallest dPMMA chains (20 000 g mol⁻¹) (Fig. 2). The samples prepared

with 20 000 g mol⁻¹ dPMMA do not show a trend as a function of blend composition. The 5:95, 10:90, and 15:85 blends result in the similar extents of stratification, while the 20:80 blend has a reduced extent of stratification. Despite this result, the increase in extent of stratification for less P3HT concentrated blends is very minimal when compared to the impact P3HT concentration has in larger dPMMA molecular weight blends prepared at 209.4 rad s⁻¹ as demonstrated in the ESI.†

The P3HT volume fraction depth profiles (PVFDP) are used throughout this analysis as qualitative guides of the stratification and are obtained by transforming the scattering length density profiles derived from the neutron reflectivity multi-layer fits. The PVFDP provide crucial insight into the stratification patterns and must be examined and considered to inform our understanding of the extent of stratification patterns, especially when the observed trends are non-trivial. The PVFDP of the samples prepared with 20 000 g mol⁻¹ dPMMA at 209.4 rad s⁻¹ are shown in Fig. 3 which exhibits constant P3HT concentration throughout the entire thickness of the film for all blend compositions. Our previous work ascribes the increase in extent of stratification observed with P3HT concentration to the phase separation of the dPMMA and P3HT due to repulsive interactions between the two polymers. These repulsive interactions are consistent with a decrease in miscibility of the blend with increased loading of the P3HT, and the observed increase in stratification with P3HT concentration at the highest dPMMA molecular weights. We attribute the limited stratification of the P3HT ($M_{\rm w} \sim 20\,000\,{\rm g~mol^{-1}}$) and low molecular weight dPMMA $(20\,000 \text{ g mol}^{-1})$ films prepared at 209.4 rad s⁻¹ to an increase in P3HT and dPMMA miscibility relative to the blends that contain the larger molecular weight dPMMA (131 500 g mol⁻¹, 316 000 g mol⁻¹, 520 000 g mol⁻¹).^{29,30}

The lack of stratification in the 20 000 g mol⁻¹ dPMMA samples prepared at 209.4 rad s⁻¹ is also consistent with the lack of an entropic driving force for the smaller polymer to

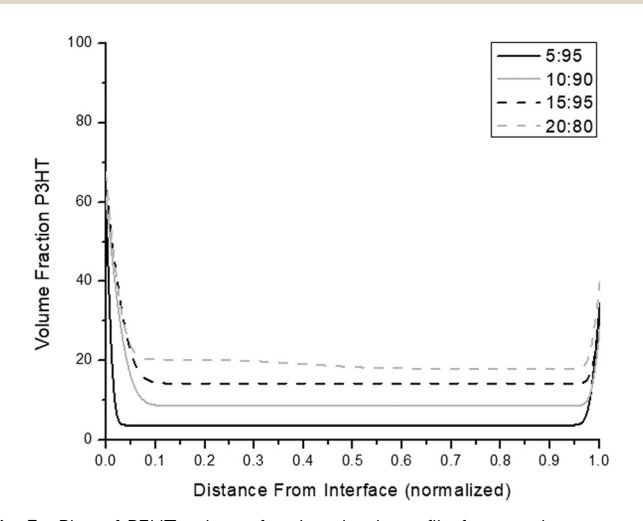


Fig. 3 Plot of P3HT volume fraction depth profile for samples prepared with 20 000 g mol^{-1} at 209.4 rad s^{-1} as a function of blend composition 5:95 (solid black), 10:90 (solid grey), 15:85 (dashed black), and 20:80 (dashed grey).

segregate to the surface as both polymers in this blend have very similar chain lengths. This result indicates that the molecular weight dependence of the blend miscibility regulates the impact of the P3HT concentration on the extent of stratification. For example, the extent of stratification for blends with $20\,000~{\rm g~mol}^{-1}$ dPMMA is not strongly dependent on the P3HT concentration, while the extent of stratification for samples with the larger dPMMA molecular weights vary significantly with P3HT concentration. Therefore, the difference in molecular weight between P3HT and dPMMA is required in order for the enthalpic/surface energy/blend miscibility driving forces to regulate the extent of stratification of the final film.

52.4 rad s⁻¹ casting speed

To understand the impact of blend composition and molecular weight on the extent of stratification at the slowest film formation time, all dPMMA molecular weights and blend compositions were prepared at 52.4 rad s⁻¹. The extents of stratification of these samples are plotted as a function of the dPMMA molecular weight in Fig. 4. The impact of dPMMA molecular weight on the extent of stratification for samples prepared at 52.4 rad s⁻¹ is less clear relative to the impact of dPMMA molecular weight for samples prepared at the two faster casting speeds. The stratification of the blend composition of 5:95 increased steadily with the dPMMA molecular weight, while the other compositions exhibit an increase in extent of stratification at low dPMMA molecular weight but remain constant or decrease for the two largest dPMMA molecular weights.

The impact of P3HT concentration on the extent of stratification is slightly clearer than the impact of molecular weight for the samples prepared at 52.4 rad s⁻¹. Nonetheless, the impact of P3HT concentration on the extent of stratification is not trivial for the polymer blend films prepared at 52.4 rad s^{-1} . As P3HT concentration increases in the blend, the extent of stratification increases for samples prepared with either

5:95 52.4 rad/s 100 10:90 52.4 rad/s 15:95 52.4 rad/s 20:80 52.4 rad/s 80 Extent of Stratification 100000 200000 300000 400000 500000 dPMMA Molecular Weight (g/mol)

Fig. 4 Plot of extent of stratification as a function of dPMMA molecular weight, and blend composition 5:95 (stars), 10:90 (circles), 15:85 (crosses), and 20:80 (triangles) all prepared at 52.4 rad s $^{-1}$.

20 000 g mol⁻¹ and 131 000 g mol⁻¹ dPMMA molecular weights, but the behavior of the samples prepared with 316 000 g mol⁻¹ and 520 000 g mol⁻¹ dPMMA are more complex. Investigating the stratification of the 316 000 g mol⁻¹ and 520 000 g mol⁻¹ dPMMA samples prepared at 52.4 rad s⁻¹ independently may aid in elucidating the driving forces that guide the extent of stratification when these samples are prepared at this casting speed. The extent of stratification as a function of casting speed for dPMMA molecular weights of 316 000 g mol⁻¹ (Fig. 5) is discussed first, followed by the discussion of the 520 000 g mol⁻¹ (Fig. 8) and 20000 g mol⁻¹ (Fig. 10) samples. The extent of stratification for samples containing 131 500 g mol⁻¹ dPMMA as a function of casting speed can be referenced in Fig. 1b.

316 000 g mol⁻¹ dPMMA. All P3HT:316k dPMMA samples, displayed in Fig. 5, show an increase in extent of stratification as a function of decreased casting speed except for the sample prepared with a blend ratio of 20:80. The 20:80 films experience the largest extent of stratification when prepared at 104.7 rad s⁻¹, while all the other blend compositions result in the largest extents of stratification when prepared at the slowest casting speed, 52.4 rad s^{-1} . Regardless of blend composition, decreasing the casting speed from 209.4 to 104.7 rad s⁻¹ results in an increase in extent of stratification, where the difference in extent of stratification between samples prepared at 104.7 rad s⁻¹ and 209.4 rad s⁻¹ is quite large. The increase in the extent of stratification in the films when decreasing the casting speed from 104.7 rad s⁻¹ to 52.4 rad s⁻¹ results in smaller, if any, increases for all the blend compositions except for the 20:80 blend. Apart from the differences in extent of stratification observed at each casting speed, all blend compositions exhibit a correlation to the concentration of P3HT in the blend, where an increase in P3HT concentration results in an increase in the extent of stratification. The only discrepancy from this trend is the extent of stratification observed for the 20:80 sample prepared at 52.4 rad s⁻¹.

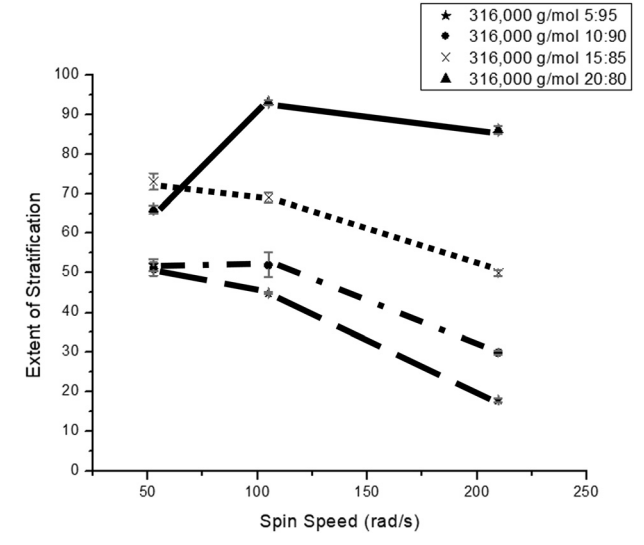


Fig. 5 Plot of extent of stratification as a function of spin cast speed, and composition 5:95 (stars), 10:90 (circles), 15:85 (crosses), and 20:80 (triangles) all prepared with 316 000 g mol^{-1} dPMMA.

Soft Matter Paper

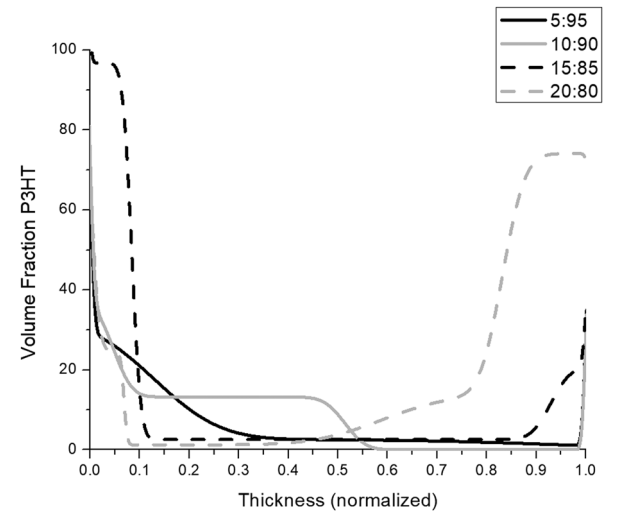


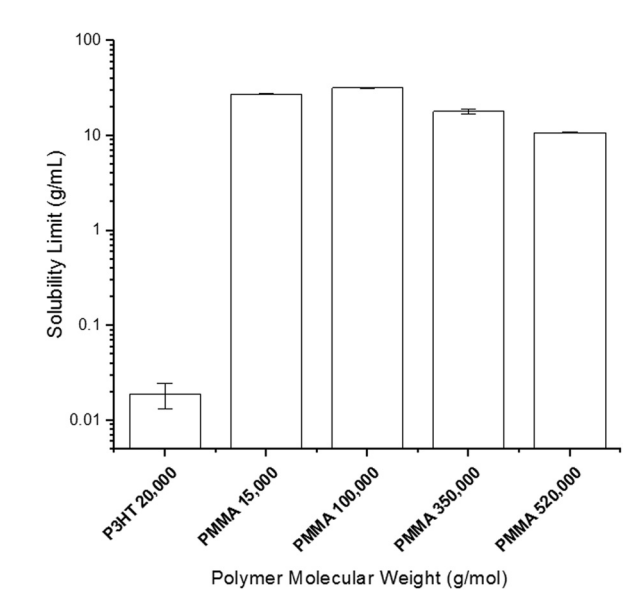
Fig. 6 Plot of P3HT volume fraction depth profile for samples prepared with 316 000 g mol^{-1} at 52.4 rad s^{-1} as a function of blend composition 5:95 (solid black), 10:90 (solid grey), 15:85 (dashed black), and 20:80 (dashed grev).

In the blend thin films that contain 316 000 g mol⁻¹ molecular weight dPMMA, the extent of stratification does not clearly correlate to the P3HT concentration in the blend. The blend compositions that exhibit the smallest extent of stratification are the 5:95 and 10:90 samples ($\sim 50\%$) followed by the 20:80 film (66%) and finally, 15:85 (73%). To understand this non-linear behavior, unlike the stratification of the samples that contain $20\,000\,\mathrm{g}\,\mathrm{mol}^{-1}$ and $132\,000\,\mathrm{g}\,\mathrm{mol}^{-1}$ dPMMA, the PVFDP of these films must be inspected (Fig. 6).

Inspection of Fig. 6 shows that the blends composed of 5:95 and 10:90 have P3HT rich layers at the air interface, while the 15:85 and 20:80 blends have P3HT rich layers at both interfaces. The blend containing 15:85 P3HT:316 000 g mol⁻¹ dPMMA has a thin layer of nearly pure P3HT at the air interface, while the P3HT in the layer at the silicon interface is not the majority component. The blend containing 20:80, on the other hand, has a highly concentrated P3HT layer at the silicon surface, while the P3HT layer at the air interface contains a lower concentration of P3HT.

A P3HT rich layer forming at the Si interface is unexpected based on the thermodynamic properties of the film, including the entropic driving forces and surface energy. The surface energy and molecular weight of P3HT is much lower than that of dPMMA in these blends. If the surface energy was the dominant driving force responsible for stratification, P3HT would segregate to the air interface. Additional driving forces for stratification must be considered to explain the P3HT rich layer at the Si surface when this blend of P3HT:dPMMA is prepared at 52.4 rad s^{-1} .

As the casting speed is decreased during film fabrication, the film formation time increases due to slower solvent evaporation times. As solvent evaporates, the concentration of solids dissolved in solvent increases until the final film formation. At a certain point in the solvent evaporation process, the solubility limit of a



Solubility of the polymers utilized in this study in chlorobenzene.

polymer is reached, and the polymer precipitates. At fast casting speeds, the precipitation of the polymer and the final film formation appear to occur nearly simultaneously, and the solubility limit of the polymer does not appear to impact the film structure. However, as the casting speed decreases, the amount of time between the precipitation of the polymer and the final film formation increases. Since we only observe P3HT formation at the Si surface at the slowest casting speed, it seems reasonable that the relative solubility limits need to be considered for these slow casting speeds.

The solubility for all the polymers in the casting solvent (chlorobenzene) used in this study were experimentally determined and are plotted in Fig. 7. The solubility limit of P3HT in chlorobenzene (16 mg mL⁻¹) is three orders of magnitude less than the solubility of all the dPMMA samples in chlorobenzene (10-32 g mL⁻¹ depending on molecular weight). It is important to note that the solubility of each polymer is well above the solution concentrations used to cast the thin films and prior to spin casting, i.e. both polymers are fully dissolved in chlorobenzene in the pre-casting solution. Despite this fact, spin casting drives solvent evaporation, leading to an increase solid concentration during spin coating, where the polymer concentration crosses the solubility limit of each polymer during deposition. Since P3HT is less soluble in chlorobenzene, P3HT reaches its solubility limit first. We therefore attribute the formation of P3HT rich layers at the Si interface for samples containing P3HT: dPMMA 15:85 and 20:80 to the large differences in the solubility limits of dPMMA and P3HT in chlorobenzene. During the casting process and solvent evaporation, P3HT reaches its solubility limit prior to dPMMA. Once the solubility limit is reached, P3HT precipitates from solution, and forms a layer of P3HT at the silicon surface. This interpretation is consistent with the fact that the P3HT rich layer at the Si surface transpires for samples with higher concentrations of P3HT. These blends reach the solubility limit more quickly than the lower concentration

blends at the same casting speed. The precipitation of P3HT

initiates a phase separation for the otherwise miscible blend solutions resulting in the P3HT rich layer found at the Si interface for the blends with higher P3HT concentration. This precipitation results in increased extents of stratification relative to the blends containing a lower P3HT concentration.

Soft Matter

Additionally, the formation of a thin P3HT layer at the silicon substrate masks the surface energy of the substrate (becoming similar to P3HT) leading to a drastic increase in the apparent surface energy of the substrate. This change in substrate surface energy further drives P3HT towards the Si surface, in addition to the otherwise preferred air interface. The simultaneous driving forces that sequester the P3HT to both air and silicon interfaces results in smaller extents of stratification for samples prepared at 52.4 rad s⁻¹ when the solubility limit is reached prior to final film formation.

520 000 g mol⁻¹ dPMMA. Samples containing P3HT: $520\,000 \text{ g mol}^{-1} \text{ dPMMA (Fig. 8)}$ prepared at 104.7 rad s⁻¹ and 209.4 rad s⁻¹ exhibit an increase in extent of stratification as a function of increasing P3HT concentration in the blend. However, an increase in P3HT concentration for samples prepared at 52.4 rad s⁻¹ does not result in an increase in extent of stratification. In fact, the extent of stratification decreases for samples prepared at 52.4 rad s⁻¹ relative to samples prepared at 104.7 rad s⁻¹ for all blend compositions except the samples prepared with P3HT: dPMMA 5:95. Additionally, the previously determined impact of casting speed on extent of stratification (decrease in casting speed results in an increase in extent of stratification) is only observed for the samples prepared with 5:95 blend compositions. However, the extent of stratification does increase as the casting speed decreases from 209.4 rad s⁻¹ to 104.7 rad s⁻¹ for all the blend compositions, but when the samples are prepared at 52.4 rad s⁻¹, a further increase in extent of stratification is not observed for blend compositions of 10:90, 15:85, and 20:80.

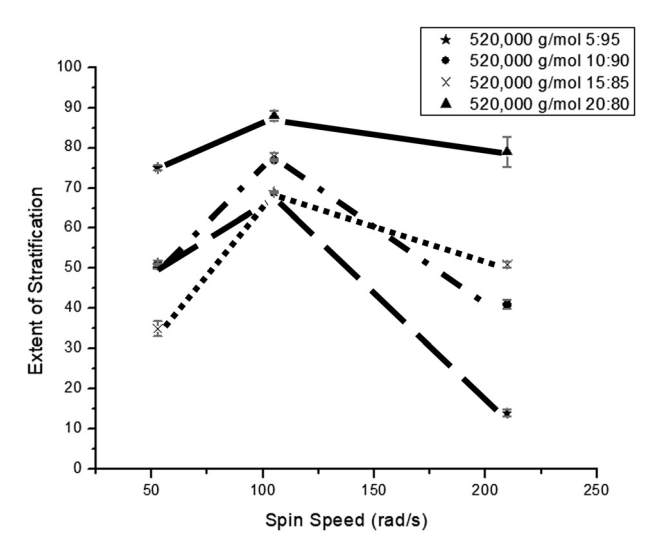


Fig. 8 Plot of extent of stratification as a function of spin cast speed, and blend composition 5:95 (stars), 10:90 (circles), 15:85 (crosses), and 20:80 (triangles) all prepared with 520 000 g mol^{-1} dPMMA.

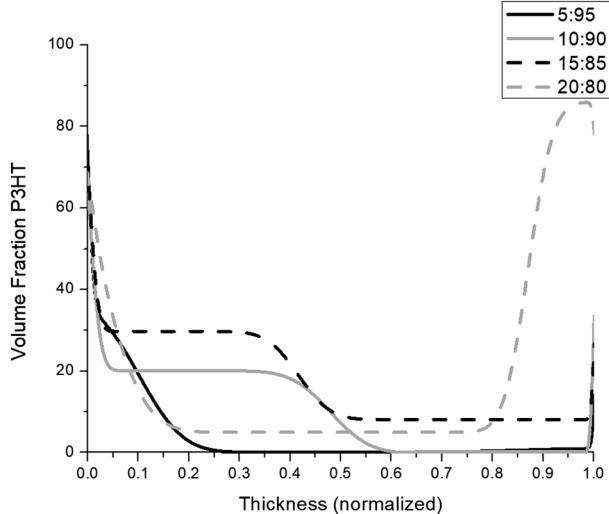


Fig. 9 Plot of P3HT volume fraction depth profiles for samples prepared with 520 000 g mol⁻¹ at 52.4 rad s⁻¹ as a function of blend composition 5:95 (solid black), 10:90 (solid grey), 15:85 (dashed black), and 20:80 (dashed grey).

To utilize the same analysis process as above, the PVFDP of the thin film blends that include 520 000 g mol⁻¹ dPMMA prepared at 52.4 rad s⁻¹ are provided in Fig. 9. Unlike the samples prepared with 316 000 g mol⁻¹ dPMMA, the blend composition resulting in the largest extent of stratification is 5:95 (75%) followed by 20:80 and 10:90 having almost the same extent of stratification (51%) and finally, 15:85 has the lowest extent of stratification (35%).

The P3HT rich layer organizes at the air interface for the sample containing 5:95 and it is the only sample with this structure. The blend composition of 20:80 is comprised of a P3HT rich layer at the air interface, as well as at the silicon substrate. The 20:80 sample is the only sample where a P3HT rich layer is found at the Si substrate. The middle two blend compositions (10:90 and 15:85) exhibit similar stratification patterns to one another where the P3HT rich layer seems to broaden into the middle bulk of the film. The P3HT layer accumulating at the silicon substrate is explained by the premature precipitation of P3HT occurring prior to film formation, yet the reason that the P3HT extends into the bulk of the film is less understood. This middle layer is found in the top half of the film closest to the air interface, consistent with the stratification of P3HT towards the air interface. As mentioned above, the precipitation of P3HT during the deposition process appears to be an important process in the development of the stratification of slowly formed blend films. In this process, the precipitated P3HT must also diffuse though the solvated dPMMA to reach the silicon substrate. The rate at which P3HT diffuses through solvated dPMMA is dictated by the size of the dPMMA chains, where the diffusion of the P3HT chains through a larger dPMMA matrix will be slower than its diffusion through a smaller matrix.

The slower diffusion of P3HT through the 520 000 dPMMA matrix manifests as the broadening of the P3HT concentration profile in the middle of the film rather than at the silicon

Soft Matter Paper

surface. Additionally, the inability of P3HT to phase separate from dPMMA leads to a decrease in the extent of stratification for the higher concentration P3HTR samples. The coupling of this precipitation to the entropic and enthalpic driving forces for stratification results in a complex process that is difficult to control for the high chain length dPMMA samples. However, these results do reveal the importance of considering the solubility limits of the polymers in the pre-deposition solvent, especially when the polymer with the lower solubility limit is the polymer with the smallest surface energy.

20 000 g mol⁻¹ dPMMA. The solubility limits of P3HT interfered with the extent of stratification as a function of casting speed trends for samples prepared with 316 000 g mol⁻¹ and 520 000 g mol⁻¹ dPMMA at slow casting speeds, while at fast casting speeds, the improved miscibility of 20 000 g mol⁻¹ P3HT and 20 000 g mol⁻¹ dPMMA inhibited stratification as well. To complete this study, the extent of stratification of the 20 000 g mol⁻¹ dPMMA blend as a function of casting speed is also analyzed and is shown in Fig. 10.

The samples prepared with a blend composition of P3HT:20 000 g mol⁻¹ dPMMA 5:95 result in an increase in extent of stratification as casting speed increases (Fig. 10). The blend composition of 10:90 results in a relatively constant extent of stratification around 35%, for the slowest casting speeds, but when prepared at the fastest casting speed, a reduction in the extent of stratification occurs. The samples prepared with blend compositions of 15:85 and 20:80 result in a drastic increase in extent of stratification when the casting speed is decreased from 209.4 rad s^{-1} to 104.7 rad s^{-1} . The blend composition of 20:80 does not experience a change in the extent of stratification as the casting speed is decreased from 104.7 rad s⁻¹ to 52.4 rad s⁻¹, yet the blend composition of 15:85 experiences a decrease in extent of stratification when changing the casting speed from 104.7 rad s⁻¹ to 52.4 rad s⁻¹. The 15:85 blend composition obtains the largest extent of stratification (60%) occurring when prepared at 104.7 rad s⁻¹,

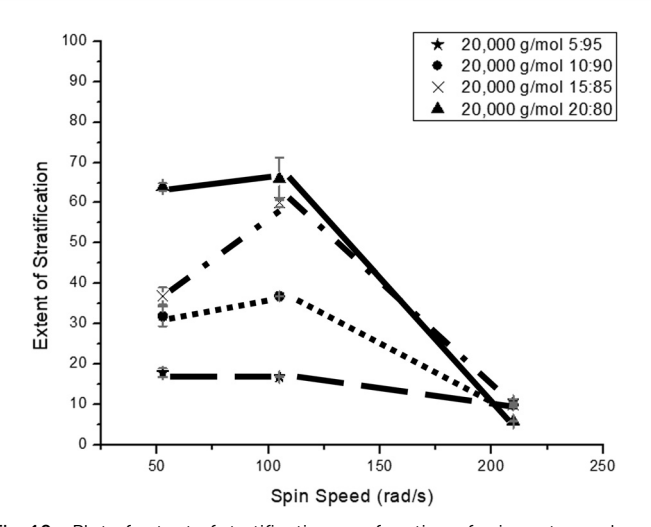


Fig. 10 Plot of extent of stratification as a function of spin cast speed, and blend composition 5:95 (stars), 10:90 (circles), 15:85 (crosses), and 20:80 (triangles) all prepared with 20 000 g mol^{-1} dPMMA.

approximately 20% larger than the extent of stratification for this sample prepared at 52.4 rad s⁻¹. For the samples containing 20 000 g mol⁻¹ dPMMA, the influence of P3HT concentration in the blend is dependent on the casting speed. When samples are prepared at 52.4 rad s^{-1} or 104.7 rad s^{-1} , an increase in P3HT concentration leads to an increase in extent of stratification. Contrarily, when samples are prepared at 209.4 rad s⁻¹, the impact of P3HT concentration on the extent of stratification is unclear.

To understand these trends, the PVFDP are analyzed. The PVFDP for samples containing 20 000 g mol⁻¹ dPMMA prepared at 209.4 rad s^{-1} are shown in Fig. 3 and the PVFDP for the same samples prepared at 52.4 rad s^{-1} and 104.7 rad s^{-1} are displayed in Fig. 11a and b. In the depth profiles for samples prepared at the slowest spin speed, 52.4 rad s^{-1} , P3HT rich layers are found near the air interface that extend into the middle of the film for the 5:95 and 10:90 blend compositions. The 15:85 and 20:80 blend compositions form a P3HT rich layer at the silicon interface. It is interesting that even though the P3HT rich layers do not form at the same air or silicon interface, the extents of stratification for each of these blend compositions appears to increase with the concentration of P3HT in the blend. This result emphasizes that only looking at the extent of stratification for a specific sample does not describe the stratification completely. The P3HT layers formed at the silicon substrate for the highest blend compositions are ascribed to the precipitation of P3HT prior to film formation. The extent of stratification is largest for the samples cast at 104.7 rad s⁻¹, rather than the samples cast with the slowest casting speed. The precipitation of P3HT competes with the entropic and surface energy factors driving P3HT to the air interface for samples cast at the slowest casting speeds and although the extent of stratification is larger for films formed at slightly higher speeds, the precipitation may also play a role in the stratification of films formed at slightly faster spin speeds as well. For samples with $20\,000~g~mol^{-1}$ prepared at $104.7~rad~s^{-1}$ (Fig. 11b), the P3HT layers are only found at the air interface but show either two P3HT rich layers with varying concentrations, or a P3HT rich layer with broad interface (gradual change in concentration) into the PMMA rich layer for the 10:90, 15:85, and 20:80 blends. This is consistent with the segregation of the P3HT to the air interface, combined with the precipitation of P3HT during film formation, but the impact of this precipitation is less apparent than the samples prepared at a slower casting speed and longer film formation time. The precipitation of P3HT competes with the forces responsible for driving P3HT to the air interface which may decrease the extent of stratification measured for these samples.

131 500 g mol⁻¹ dPMMA. The highly concentrated P3HT blend compositions prepared with 20 000 g mol⁻¹, 316 000 g mol⁻¹, and 520 000 g mol⁻¹ dPMMA exhibit P3HT precipitation when prepared at the slowest casting speed, 52.4 rad s⁻¹. Fig. 12 compares the PVFDP of samples consisting of 131 500 g mol⁻¹ dPMMA prepared at 52.4 rad s⁻¹. Regardless of blend composition, all samples stratify to form P3HT rich layers at the air interface. As with the 20 000 g mol⁻¹ samples prepared at 104.7 rad s⁻¹, the

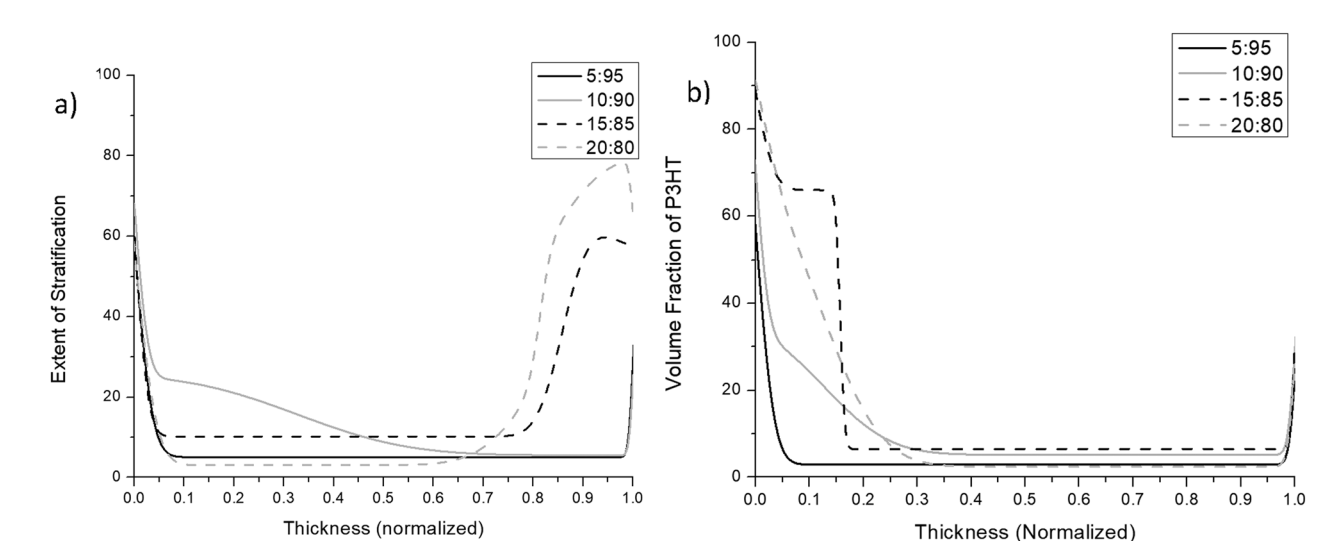


Fig. 11 Plots of P3HT volume fraction depth profiles for samples prepared with 20 000 g mol^{-1} at (a) 52.4 rad s^{-1} and (b) 104.7 rad s^{-1} as a function of blend composition 5:95 (solid black), 10:90 (solid grey), 15:85 (dashed black), and 20:80 (dashed grey).

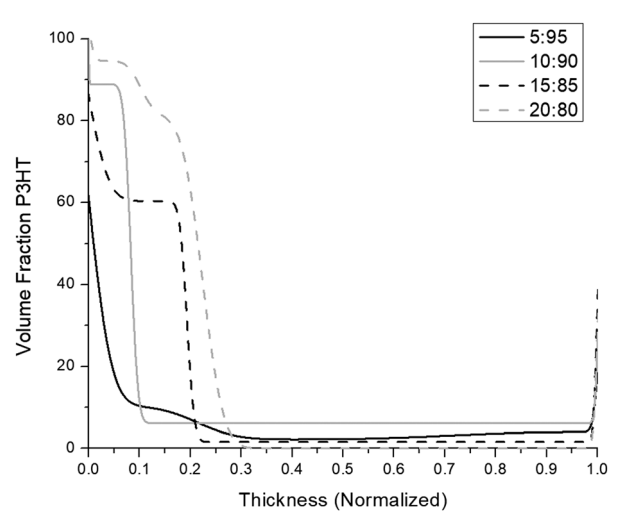


Fig. 12 Plot of P3HT volume fraction depth profiles for samples prepared with $131500 \text{ g mol}^{-1}$ at 52.4 rad s^{-1} as a function of blend composition 5:95 (solid black), 10:90 (solid grey), 15:85 (dashed black), and 20:80 (dashed grey)

P3HT rich layers at the air interface show two to three distinct P3HT rich layers each with different P3HT concentrations. This is consistent with P3HT precipitation where its segregation to the Si surface is attenuated by other driving forces (i.e. lower surface energy and smaller molecular weight) that pull P3HT to the air interface. The fact that the 131 500 dPMMA is a longer chain than the P3HT in this samples means that there is a larger entropic driving force for the P3HT to go to the air surface than in the 20 000 dPMMA samples. This larger entropic driving force competes with the segregation of the P3HT to the Si surface that is driven by the P3HT precipitation, where this competition results in a layering of the P3HT in the film, but no segregation at the Si surface.

Since the entropic driving force for P3HT to stratify at the air interface increases with larger molecular weight dPMMA,

the influence of the P3HT solubility limit on the stratification therefore decreases with increasing dPMMA chain length. These results indicate that the entropic driving forces and the influence of the P3HT solubility compete in the stratification process, and to control the stratification of polymer blends, these two driving forces must be understood and controlled when films are prepared at slow casting speeds and long film formation times.

Conclusion

Polymer blend thin film depth profiles were obtained through neutron reflectivity experiments of spin cast P3HT/dPMMA blend thin films. The results presented in this paper indicate a hierarchy of driving forces that control the film vertical profile, where there appears to be a coupling of the thermodynamic and kinetic factors that influence film morphology. At high spin rates and thus films that are formed very quickly, the immiscibility of the blend is the dominant driving force in the stratification of the polymer blend. More specifically, the stratification of the components is driven by the relative surface energies of the polymers in the blend. As the casting speed decreases and film formation time increases, the immiscibility and surface energy contrast between the two polymers still drives the vertical stratification, but entropic driving forces, which are related to the relative molecular weight of the two polymers, become important in the stratification process. This competition of multiple factors manifests the most at the slowest casting speed and longest film formation times, where the polymer-polymer miscibility, relative surface energies, and entropy of the two polymers in the thin film simultaneously dictate the extent of stratification. Moreover, at these longer film formation times, the solubility limits of the two polymers in the pre-deposition solvent also play a role in the final film structure. As the casting speed is decreased, the time between precipitation of the solid polymers from solution and the film

Soft Matter Paper

completion increases. Once a polymer has reached its solubility limit during the casting process, further stratification of that polymer is now impeded.

The entirety of these results indicate that the dominant thermodynamic driving force driving the stratification of P3HT:dPMMA thin films is the immiscibility of the polymer blend. Yet by intelligently altering the kinetics and balancing the thermodynamic properties controlled by the polymer blend composition and polymer molecular weight, the extent of stratification and depth profiles can be tailored. Although these results isolate the relative importance of individual thermodynamic parameters, the results reported here provide insight into the kinetic factors that couple to the important thermodynamic properties (entropy, enthalpy, solubility, miscibility) and impact the stratification of a polymer blend.

In these studies, the least amount of stratification was observed when the two polymers were the most miscible, which occurs for the blend containing the two smallest molecular weights. According to the results in this manuscript, to maximize the amount of stratification of a sample, as well as acquire a sharp interface between the stratified layers, the surface energy difference and variation in quantity of chain ends between the polymers should be maximized. However, it should be noted that for these P3HT:PMMA blends, the P3HT always has the lowest molecular weight and smallest surface energy. The conclusions outlined in this paper may be applied to other systems where the lowest molecular weight polymer also has the smallest surface energy because these thermodynamic properties drive the polymer to the air interface. Additional experiments are required to understand the balance between surface energy and entropic driving forces in stratification of polymer blends where the lowest surface energy polymer has a significantly higher molecular weight.

Although these results monitored the behavior of P3HT:dPMMA, polymer blends that are suitable for organic transistors where a sharp interface is desirable, these results also provide a fundamental understanding of the coupling of thermodynamic and kinetic factors in the film formation process to create a less stratified film, for instance if a blend thin film that were to be used in bulk heterojunction devices. Moreover, this fundamental understanding provides insight that can be used to rationally design one step solution processing protocols of a multitude of polymer blends where the targeted stratification for the application is known.

Conflicts of interest

There are no conflicts to declare.

Acknowledgements

MDD acknowledges the support of the U.S. Department of Energy, Office of Science, Basic Energy Sciences, Materials Sciences and Engineering Division. SJR was supported by the National Science Foundation (DMR-1409034 and DMR-1808946)

for this project. We acknowledge the support of the National Institute of Standards and Technology, U.S. Department of Commerce, in providing the neutron research facilities used in this work.

References

- 1 D. B. Hall, P. Underhill and J. M. Torkelson, Spin Coating of Thin and Ultrathin Polymer Films, Polym. Eng. Sci., 1998, 38(12), 2039–2045, DOI: 10.1002/pen.10373.
- 2 D. Meyerhofer, Characteristics of Resist Films Produced by Spinning, J. Appl. Phys., 1978, 49(7), 3993-3997, DOI: 10.1063/ 1.325357.
- 3 J. H. Lai, An Investigation of Spin Coating of Electron Resists, Polym. Eng. Sci., 1979, 19(15), 1117-1121, DOI: 10.1002/pen.760191509.
- 4 A. D. F. Dunbar, P. Mokarian-Tabari, A. J. Parnell, S. J. Martin, M. W. A. Skoda and R. A. L. Jones, A Solution Concentration Dependent Transition from Self-Stratification to Lateral Phase Separation in Spin-Cast PS:D-PMMA Thin Films, Eur. Phys. J. E: Soft Matter Biol. Phys., 2010, 31(4), 369-375, DOI: 10.1140/epje/i2010-10592-4.
- 5 P. A. Chiarelli, M. S. Johal, D. J. Holmes, J. L. Casson, J. M. Robinson and H. L. Wang, Polyelectrolyte Spin-Assembly, Langmuir, 2002, 18(1), 168-173, DOI: 10.1021/la011333s.
- 6 P. A. Chiarelli, M. S. Johal, J. L. Casson, J. B. Roberts, J. M. Robinson and H.-L. Wang, Controlled Fabrication of Polyelectrolyte Multilayer Thin Films Using Spin-Assembly, Adv. Mater., 2001, 13(15), 1167-1171, DOI: 10.1002/1521-4095(200108)13:15 < 1167::AID-ADMA1167 > 3.0.CO;2-A.
- 7 T. G. Stange, R. Mathew, D. F. Evans and W. A. Hendrickson, Scanning Tunneling Microscopy and Atomic Force Microscopy Characterization of Polystyrene Spin-Coated onto Silicon Surfaces, Langmuir, 1992, 8(3), 920-926, DOI: 10.1021/la00039a030.
- 8 R. J. Kline, M. D. McGehee, E. N. Kadnikova, J. Liu, J. M. J. Fréchet and M. F. Toney, Dependence of Regioregular Poly(3-Hexylthiophene) Film Morphology and Field-Effect Mobility on Molecular Weight, Macromolecules, 2005, 38(8), 3312-3319, DOI: 10.1021/ma047415f.
- 9 Y. Shi, J. Liu, Y. Yang, Y. Shi, J. Liu and Y. Yang, Device Performance and Polymer Morphology in Polymer Light Emitting Diodes: The Control of Thin Film Morphology and Device Quantum Efficiency Device Performance and Polymer Morphology in Polymer Light Emitting Diodes: The Control of Thin Film Morphology, J. Appl. Phys., 2000, 87(9), 4254-4263, DOI: 10.1063/1.373062.
- 10 D. T. W. Toolan, A. Isakova, R. Hodgkinson, N. Reeves-Mclaren, O. S. Hammond, K. J. Edler, W. H. Briscoe, T. Arnold, T. Gough and P. D. Topham, et al., Insights into the Influence of Solvent Polarity on the Crystallization of Poly(Ethylene Oxide) Spin-Coated Thin Films via in Situ Grazing Incidence Wide-Angle X-Ray Scattering, Macromolecules, 2016, 49(12), 4579-4586, DOI: 10.1021/acs.macromol.6b00312.
- 11 B. Morgan and M. D. Dadmun, Illumination of Conjugated Polymer in Solution Alters Its Conformation and

Thermodynamics, Macromolecules, 2016, 49(9), 3490-3496, DOI: 10.1021/acs.macromol.6b00527.

Soft Matter

- 12 B. Morgan and M. D. Dadmun, Illumination Alters the Structure of Gels Formed from the Model Optoelectronic Material P3HT, Polymer, 2017, 108, 313-321, DOI: 10.1016/ j.polymer.2016.11.056.
- 13 B. Morgan and M. D. Dadmun, The Importance of Solvent Quality on the Modification of Conjugated Polymer Conformation and Thermodynamics with Illumination, Soft Matter, 2017, 13(15), 2773-2780, DOI: 10.1039/C6SM02631A.
- 14 S. Han, X. Zhuang, S. Wei, X. Yang, L. Li and J. Yu, Poly(3-Hexylthiophene)/Polystyrene (P3HT/PS) Blends Based Organic Field-Effect Transistor Ammonia Gas Sensors, Sens. Actuators, B, 2016, 225, 10-15, DOI: 10.1016/j.snb.2015.11.005.
- 15 S. Cho, N. Coates, J. S. Moon, S. H. Park, A. Roy, S. Beaupre, D. Moses, M. Leclerc, K. Lee and A. J. Heeger, Bulk Heterojunction Solar Cells with Internal Quantum Efficiency Approaching 100, Nat. Photonics, 2009, 3(5), 297–302, DOI: 10.1038/nphoton.2009.69.
- 16 C. M. Björström, A. Bernasik, J. Rysz, A. Budkowski, S. Nilsson, M. Svensson, M. R. Andersson, K. O. Magnusson and E. Moons, Multilayer Formation in Spin-Coated Thin Films of Low-Bandgap Polyfluorene:PCBM Blends, J. Phys.: Condens. Matter, 2005, 17(50), L529-L534, DOI: 10.1088/0953-8984/17/50/L01.
- 17 C. Liu, Y. Li, M. V. Lee, A. Kumatani and K. Tsukagoshi, Self-Assembly of Semiconductor/Insulator Interfaces in One-Step Spin-Coating: A Versatile Approach for Organic Field-Effect Transistors, Phys. Chem. Chem. Phys., 2013, 15(21), 7917-7933, DOI: 10.1039/c3cp44715d.
- 18 L. Kergoat, N. Battaglini, L. Miozzo, B. Piro, M. C. Pham, A. Yassar and G. Horowitz, Use of Poly(3-Hexylthiophene)/ Poly(Methyl Methacrylate) (P3HT/PMMA) Blends to Improve the Performance of Water-Gated Organic Field-Effect Transistors, Org. Electron., 2011, 12(7), 1253-1257, DOI: 10.1016/ j.orgel.2011.04.006.
- 19 B. Morgan and M. D. Dadmun, The Effect of Illumination on the Depth Profile of Thermally Annealed MEH-PPV/DPS Blends, J. Polym. Sci., Part B: Polym. Phys., 2017, 1142-1149, DOI: 10.1002/polb.24354.
- 20 T. Wang, N. W. Scarratt, H. Yi, I. F. Coleman, Y. Zhang, R. T. Grant, J. Yao, M. W. A. Skoda, A. D. F. Dunbar and

- R. A. L. Jones, et al., Vertical Stratification and Its Impact on Device Performance in a Polycarbazole Based Copolymer Solar Cells, J. Mater. Chem. C, 2015, 3(16), 4007-4015, DOI: 10.1039/C4TC02884H.
- 21 M. G. Hennessy, V. M. Burlakov, A. Münch, B. Wagner and A. Goriely, Propagating Topological Transformations in Thin Immiscible Bilayer Films, EPL, 2014, 105(6), 66001, DOI: 10.1209/0295-5075/105/66001.
- 22 A. Beaugendre, S. Degoutin, S. Bellayer, C. Pierlot, S. Duquesne, M. Casetta and M. Jimenez, Progress in Organic Coatings Self-Stratifying Coatings: A Review, Prog. Org. Coat., 2017, 110, 210-241, DOI: 10.1016/j.porgcoat.2017.03.011.
- 23 C. Schaefer, J. J. Michels and P. Van Der Schoot, Dynamic Surface Enrichment in Drying Thin-Film Binary Polymer Solutions, *Macromolecules*, 2017, **50**(15), 5914–5919, DOI: 10.1021/acs.macromol.7b01224.
- 24 J. Baghdachi, H. Perez, P. Talapatcharoenkit and B. Wang, Design and Development of Self-Stratifying Systems as Sustainable Coatings, Prog. Org. Coat., 2015, 78, 464-473, DOI: 10.1016/j.porgcoat.2014.06.017.
- 25 Y. Yan, X. Liu and T. Wang, Conjugated-Polymer Blends for Organic Photovoltaics: Rational Control of Vertical Stratification for High Performance, Adv. Mater., 2017, 29, 1601674, DOI: 10.1002/adma.201601674.
- 26 O. Wodo and B. Ganapathysubramanian, How Do Evaporating Thin Films Evolve? Unravelling Phase-Separation Mechanisms during Solvent-Based Fabrication of Polymer Blends, Appl. Phys. Lett., 2014, 105(15), 153104, DOI: 10.1063/1.4898136.
- 27 R. J. Kline, M. D. Mcgehee, M. F. Toney, S. Synchrotron and M. Park, Highly Oriented Crystals at the Buried Interface in Polythiophene Thin-Film Transistors, Nat. Mater., 2006, 5, 222-228, DOI: 10.1038/nmat1590.
- 28 S. J. Rinehart, G. Yuan and M. D. Dadmun, Elucidating the Kinetic and Thermodynamic Driving Forces in Polymer Blend Film Self-Stratification, Macromolecules, 2018, 51, 7836-7844, DOI: 10.1021/acs.macromol.8b01397.
- 29 M. Rubinstein and R. H. Colby, Polymer Physics, Oxford University Press, 2003.
- 30 P. C. Hiemenz and T. P. Lodge, Polymer Chemistry, Taylor & Francis Group, LLC, Boca Raton, FL, 2nd edn, 2007.